SHiP
Search for Hidden Particles

CERN-SHiP-NOTE-2020-002
December 7, 2020

Reconstruction of 400 GeV/c proton interactions with the SHiP-charm project

C. Ahdida[12], A. Akmete[16], A. Bay[14], C. Betancourt[15], D. Bick[3], S. Bieschke[3], W.M. Bonivento[5], A. Buonaura[15], M. Campanelli[18], M. Casolino[12], N. Charitonidis[12], M. Cristinziani[2], A. Crupano[6,b], R. de Asmundis[6], G. De Lellis[6,9,12,b], M. De Serio[4,a], D. De Simone[15], A. Di Crescenzo[6,b], H. Dijkstra[12], O. Durhan[16], E. Elikkaya[16], R. Froeschl[12], F. Fedotovs[18], V. Gentile[6,9], A. Golutvin[17,9], P. Gorbounov[12], M. Gorshenkov[9], A.L. Grandchamp[14], G.J. Haefeli[14], E. van Herwijnen[12], M. Hushchyn[11], A. Iuliano[6,b], R. Jacobsson[12], M. Jonker[12], E. Khalikov[10], N. Konovalova[8,9], A. Korzenev[13], V. Kostyukhin[2], O. Lantwin[9,15], P. Mermod[13], N. Okateva[8,9], B. Opitz[3], N. Owtscharenko[2], A. Pastore[4], F. Redi[14], A.B. Rodrigues Cavalcante[14], T. Ruf[12], A. Shakin[9], S. Shirobokov[17], S. Simone[4,a], M.E. Stramaglia[14], D. Sukhonos[12], V. Tioukov[6], G. Vankova-Kirilova[1], N. Wojcicka[12], C.S. Yoon[7]

Abstract

The SHiP-charm project was proposed to measure the associated charm production induced by 400 GeV/c protons in a thick target, including the contribution from cascade production. An optimisation run was performed in July 2018 at CERN SPS using a hybrid setup. The high resolution of nuclear emulsions acting as vertex detector was complemented by electronic detectors for kinematic measurements and muon identification. Here we present first results on the analysis of nuclear emulsions exposed in the 2018 run, which prove the capability of reconstructing proton interaction vertices in a harsh environment, where the signal is largely dominated by secondary particles produced in hadronic and electromagnetic showers within the lead target.

[1] *Faculty of Physics, Sofia University, Sofia, Bulgaria*
[2] *Physikalisches Institut, Universität Bonn, Bonn, Germany*
[3] *Universität Hamburg, Hamburg, Germany*
[4] *Sezione INFN di Bari, Bari, Italy*
[5] *Sezione INFN di Cagliari, Cagliari, Italy*
[6] *Sezione INFN di Napoli, Napoli, Italy*
[7] *Physics Education Department & RINS, Gyeongsang National University, Jinju, Korea*
[8] *P.N. Lebedev Physical Institute (LPI), Moscow, Russia*
[9] *National University of Science and Technology "MISiS", Moscow, Russia*
[10] *Skobeltsyn Institute of Nuclear Physics of Moscow State University (SINP MSU), Moscow, Russia*
[11] *Yandex School of Data Analysis, Moscow, Russia*
[12] *European Organization for Nuclear Research (CERN), Geneva, Switzerland*
[13] *University of Geneva, Geneva, Switzerland*
[14] *École Polytechnique Fédérale de Lausanne (EPFL), Lausanne, Switzerland*
[15] *Physik-Institut, Universität Zürich, Zürich, Switzerland*
[16] *Middle East Technical University (METU), Ankara, Turkey*
[17] *Imperial College London, London, United Kingdom*
[18] *University College London, London, United Kingdom*
[a] *Università di Bari, Bari, Italy*
[b] *Università di Napoli "Federico II", Napoli, Italy*

VERSION	DATE	COMMENTS
01	02.11.2020	First version
02	10.11.2020	Second version
03	07.12.2020	Third version

Contents

1 Introduction

The SHiP-charm project [1] aims at measuring the differential charm production cross section in a thick target, including the including the enhancement due to cascade production, which so far has never been measured. Elastic scattering followed by a deep inelastic interaction is the main source of increase of this process. The accurate prediction of charm hadroproduction rates is an essential ingredient to establish the sensitivity of a high-intensity proton beam dump experiment like SHiP (Search for Hidden Particles) [2] to new particles produced in charm decays and to make a precise estimation of the tau neutrino flux.

An optimization run was performed in July 2018 at the H4 beam line of CERN SPS/North Area. A thick target made of lead interleaved with nuclear emulsions was exposed to a 400 GeV/c proton-beam. The detector is a hybrid system, combining the emulsion technique with electronically-read-out detectors, a spectrometer magnet to provide the charge and momentum measurement of charmed-hadron-decay daughters and a muon identification system.

The challenge of the SHiP-charm measurement is two-fold: reconstruct tracks and interaction vertices in a high-density environment and search for rare decays of charmed hadrons. Here we focus on the identification of interaction vertices, whose success is a prerequisite for subsequent phases of the analysis.

2 Detector layout

The detector layout of the SHiP-charm experiment was optimised in order to provide full topological and kinematic reconstruction of the event. A picture of the overall setup installed in the H4-PPE134 experimental area is shown in Fig. 1.

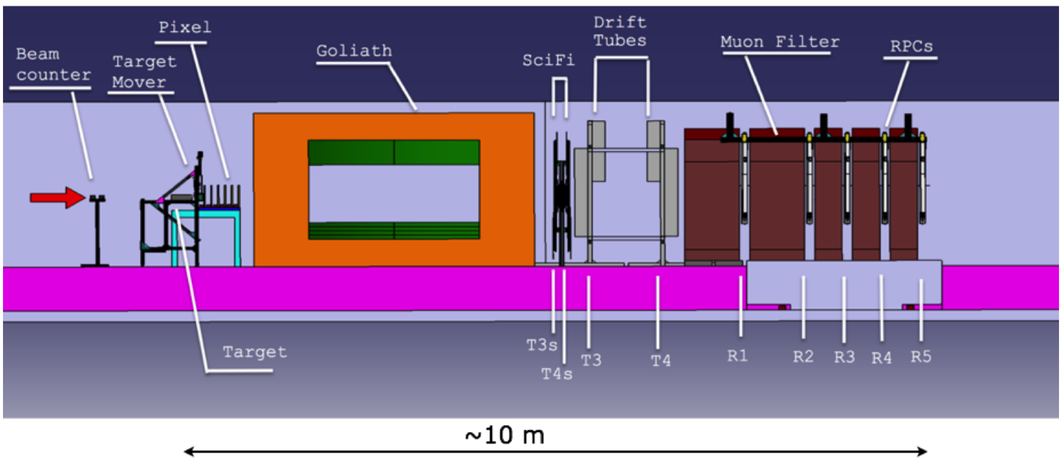

Figure 1: Lateral view of the experimental apparatus for the charm measurement. The red arrow represents the beam direction.

The topological reconstruction of proton interactions and the identification of charmed hadron decay vertices is performed within the target, which exploits the submicrometer and milliradian resolution of nuclear emulsions.

The target is constructed according to the Emulsion Cloud Chamber (ECC) technique, alternating 1 mm-thick passive material plates with emulsion films of about 330 μm thickness. The ECC was placed on a motorised mechanical stage in order to ensure a uniform distribution of the proton beam over the whole emulsion surface of 125×100 mm^2. A schematic drawing and a picture of the target mover are shown in Fig. 2. During each spill the target moves along the horizontal axis (x) at the uniform speed of 2.6 cm/s, thus covering the horizontal dimension of the ECC. Between two consecutive spills the target moves along the vertical axis (y) by 1 or 2 cm, depending on the expected track density in different target configurations. The total target surface is is consequently covered in 5 or 10 spills, respectively.

A magnetic spectrometer is located downstream of the target. The magnetic field is provided by the GOLIATH magnet [3], located in PPE134 area. In order to cope with the high multiplicity of tracks produced in each proton interaction, the upstream station is required to be highly segmented and withstand a high occupancy. Insertable B-Layer (IBL [4]) hybrid silicon pixel detectors were used for this purpose. Pixels have a size of 250×50 μm^2; pixel modules consist each of a planar sensor and two custom developed large FE-I4 front-end chips [5] with a sophisticated readout architecture. Each sensor is made of 160 columns and 336 rows, resulting in 53760 pixels. The pixel tracking station is made of six planes equipped with IBL double-chips modules. Every second plane is rotated by 90° in order to provide a 50μm position accuracy in both coordinates. The upstream station covers a transverse area of about 33.6×37.0 mm^2, sufficient to contain the beam spot and proton interaction products passing through the lead-emulsion target.

The downstream station is made by a combination of two different technologies: Scintillating fibers (SciFi) (T3s and T4s) in the central 40×40 cm^2 region, where the track density is higher, and drift tubes (T3 and T4) in the outer region. T3s and T4s stations consist each of four detection planes to provide XU and YV coordinates, where U and V planes have a stereo angle of $\sim$2.5° with respect to X an Y, respectively. Each detector plane is made by 3×12 cm-wide mats of scintillating fibers [6]. A mat is a matrix structure consisting of six staggered fibre layers with a horizontal pitch of 270 μm and a total length of 40 cm.

While the SciFi stations were built for the purpose of this measurement, drift tube chambers were adapted from modules built for the OPERA experiment [7]. T3 and T4 stations provide the x-coordinate information in the external region downstream of the GOLIATH magnet. Drift tube modules were installed on both sides and and above the region covered by the SciFi stations.

The most downstream component of the experiment is the Muon Filter, which is designed to identify muons with high efficiency, separating them from charged hadrons. At the same time, it has to reconstruct the muon track slope to match the corresponding track reconstructed in the upstream Magnetic Spectrometer and assign the momentum to the muon track. The muon tagger consists of five concrete slabs, two 80 cm-thick and three 40 cm-thick, acting as hadron absorber, interleaved with five Resistive Plate Chambers (RPC), acting as trackers. The transverse size of the RPC planes is 195×125 cm^2. The muon identification is done on the basis of the number of crossed layers in the detector. The RPCs were designed and constructed

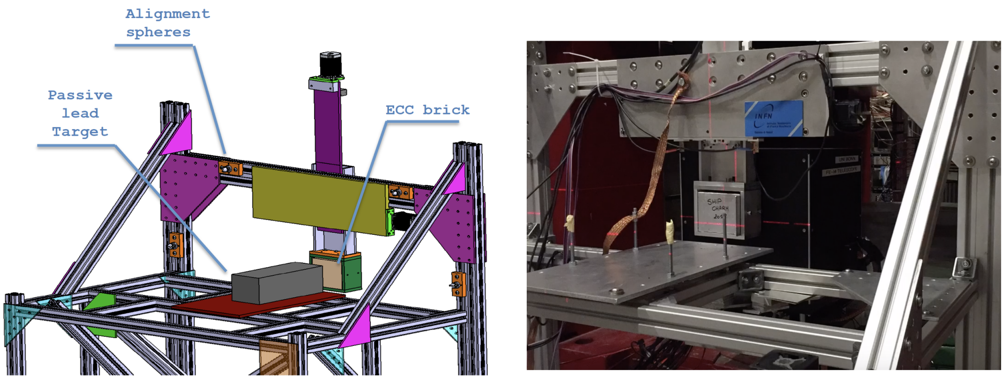

Figure 2: Left: technical drawing of the target mover. Right: picture of the mechanical stage during a test exposure of an ECC target.

to operate in avalanche mode, with a time resolution of about 1 ns. Two orthogonal sets of strips, 1 cm-wide, are used for 2D measurements with a position resolution of about 3 mm in both directions.

3 Data taking and simulation

The SHiP-charm optimisation run was performed in July 2018. The target was assembled in six different configurations in order to study the production of charmed hadrons at different depths, up to a total thickness of 280 mm, corresponding to about 1.6 interaction lengths.

The most downstream section of the target is instrumented with nuclear emulsions (the ECC) and moved by the motorised stage.

Upstream of the ECC, lead blocks with lengths from 28 to 244 mm are positioned to act as a pre-shower, according to the scheme shown in Fig. 3. Hereafter the six target configurations will be referred to as CHARMx, with x ranging from 1 to 6.

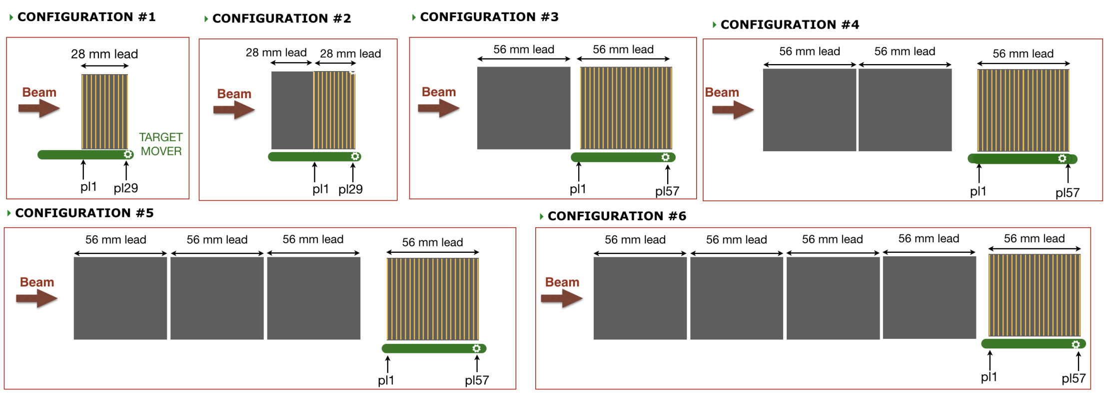

Figure 3: Schematic layout of the six target configurations.

The ECC target of CHARM1 and CHARM2 is made of a sequence of 29 emulsion films alternated with 28 passive layers, while for configurations from CHARM3 to CHARM6 it consists of 57 emulsion films and 56 passive layers. Multiple runs were performed for the different configurations in order to accumulate enough statistics in each portion of the target. A total number of 15.6×10^5 p.o.t. was integrated during the whole exposure.

All runs used lead as passive material, except for the sixth run of CHARM1, which which used 1 mm-thick tungsten layers. The composition of each configuration, the number of runs and the number of integrated p.o.t. are summarised in Tab. 1.

Configuration	n Runs	Pre-shower	ECC	n Films	integrated p.o.t. $[10^5]$
CHARM 1	6	/	28 mm Pb(W) + 29 films	174	5.4
CHARM 2	6	28 mm Pb	28 mm Pb + 29 films	174	5.2
CHARM 3	3	56 mm Pb	56 mm Pb + 57 films	171	1.0
CHARM 4	3	113 mm Pb	56 mm Pb + 57 films	171	0.8
CHARM 5	3	168 mm Pb	56 mm Pb + 57 films	171	1.6
CHARM 6	3	224 mm Pb	56 mm Pb + 57 films	171	1.6
TOTAL	24			1032	15.6

Table 1: Summary of the SHiP-charm 2018 exposure.

A total amount of 1032 emulsion films were used, corresponding to $\sim$12 m^2. The emulsions were produced by Nagoya University and Slavich Company in June 2018. Emulsion films consist of two 70 µm-thick layers of nuclear emulsion, separated by a 175 µm-thick plastic base. The transverse size is 125×100 mm^2. ECC targets were assembled in a dedicated facility at CERN right before the exposure. The exposure was performed at room temperature. After the exposure targets were transferred to the CERN facility, disassembled, and emulsion films underwent chemical treatment.

The proton beam intensity was measured by a beam counter located upstream of the target region. The temporal structure of the beam was consistent during the whole exposure, with a spill duration of 4.8 s. Its intensity, however, showed fluctuations from 7.7×10^3 to 13.8×10^3 protons/spill. The profile of the beam during the spill was monitored by the pixel station. The beam profile recorded in one spill is shown in Fig. 4. The beam spot integrated during the spill has a transverse size of about 6×15 mm^2. The elliptical shape is due to a translation of the beam center-of-gravity within the spill.

The SHiP-charm experimental apparatus was reproduced within the FairShip software, the official SHiP simulation framework derived from FairRoot [8], as shown in Fig. 5. The geometry and the position of different sub-detectors were set taking into account measurements performed in situ by the CERN survey team. The magnetic-field map measured by the CERN staff in 2017 [3] was imported in the simulation of the GOLIATH magnet.

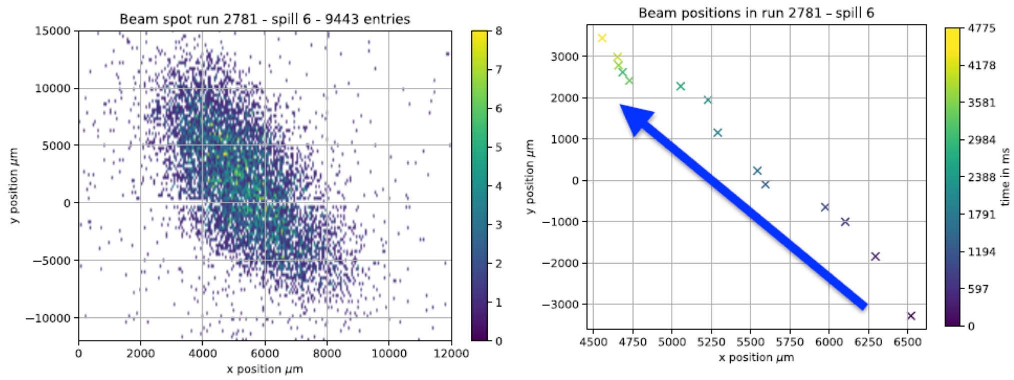

Figure 4: Left: beam profile in the transverse plane, as registered by the pixel detector in the sixth spill of CHARM2-RUN1. Right: position of the beam center-of-gravity as function of time during the spill.

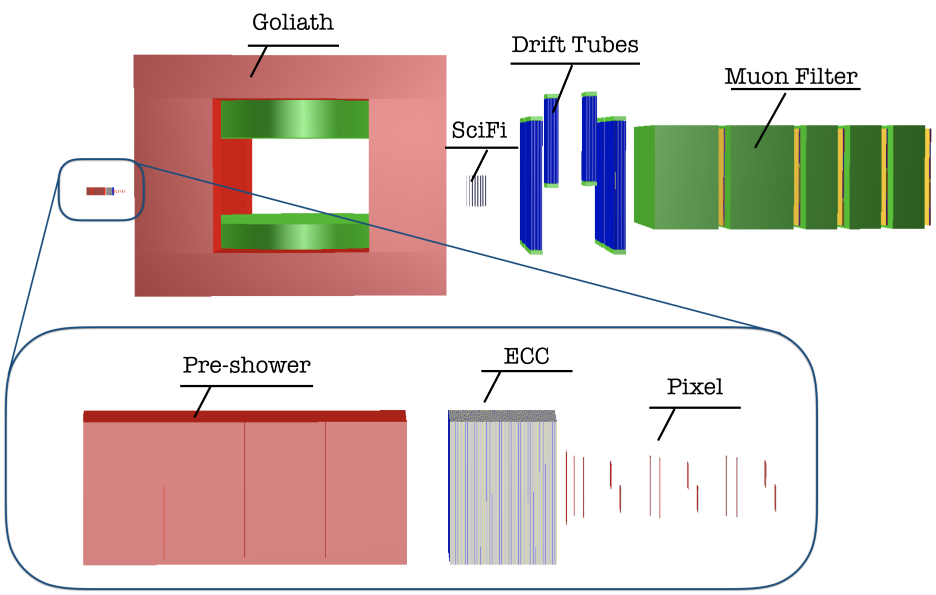

Figure 5: Layout of the SHiP-charm experimental layout, as implemented in FairShip.

The simulation of 400 GeV/c proton interactions within the target and the propagation of particles in detector materials is performed with GEANT4 [9]. Different simulation campaigns were performed in order to reproduce the six target configurations.

4 Data analysis

4.1 Track reconstruction in nuclear emulsions

The track left by a charged particle on an emulsion layer is recorded by a series of sensitised AgBr crystals, growing up to 0.6 μm diameter during the development process. Optical microscopes analyse the whole thickness of the emulsion, acquiring tomographic images at equally spaced depths. The acquired images are digitized, then an image processor recognizes the grains as *clusters*, i.e. groups of pixels of given size and shape. Thus, the track in the emulsion layer (usually referred to as *micro-track*) is obtained connecting clusters belonging to different levels, as shown in the left panel of Fig. 6. Since an emulsion film is formed by two emulsion layers, the connection of the two micro-tracks through the plastic base provides a reconstruction of the particle's trajectory in the emulsion film, called *base-track*. The reconstruction of particle tracks in the full volume requires connecting base-tracks in consecutive films. In order to define a global reference system, a set of affine transformations has to be computed to account for the different reference frames used for data taken in different films.

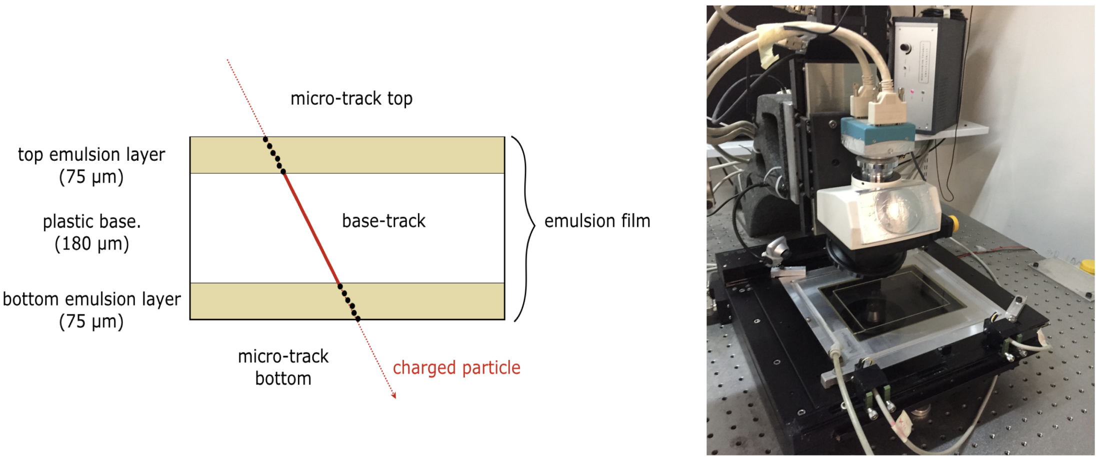

Figure 6: Left: schematic layout of a nuclear emulsion film. Right: one of the optical microscopes used for the analysis of nuclear emulsions exposed in the SHiP-charm project.

Once all emulsion films are aligned, *volume-tracks* (i.e., charged tracks which crossed several emulsion films) can be reconstructed. The track finding and fitting is based on the Kalman Filtering algorithm and takes into account possible inefficiencies in the base-track reconstruction [10].

The vertex identification is initiated by two-track vertices defined according to minimal distance criteria. Topological cuts are used in order to reduce the combinatorial background. The final selection on the track pairs is based on a vertex probability calculated with the full covariance matrix of the involved tracks. Starting from pairs, n-tracks vertices are constructed using the Kalman Filtering technique. The off-line reconstruction tool used in the analysis reported in this document is FEDRA (Frame-work for Emulsion Data Reconstruction and Analysis) [11], an object-oriented tool based on C++ language and developed in the ROOT [12] framework.

The analysis of emulsion films was performed in dedicated laboratories in Naples and Zurich equipped with a new generation of optical microscopes, one of which is shown in the right panel of Fig. 6. A recently developed upgrade of the European Scanning System (ESS) [13, 14, 15] was used. The use of a faster camera with smaller sensor pixels and a higher number of pixels combined with a lower magnification objective lens, together with a new software LASSO [16, 17] has allowed to increase the scanning speed to 180 cm^2/h [18], more than a factor ten larger than the previous generation.

4.2 Proton-beam characterisation

The number of protons impinging on ECC target units vary from $10^2/cm^2$ to $10^3/cm^2$ according to the configuration of the exposure. The data analysis shows that the track density increases with the depth in the module due to the proton interactions, hadronic reinteractions and electromagnetic showers, as shown in Fig. 7. The density of segments reconstructed in a single emulsion film extends up to $4{\times}10^4/cm^2$.

Figure 8 shows the characterisation of the proton beam in one of the ECC targets both in terms of angle (left) and position (right). The pattern observed in the position distribution reproduces the movement of the target with respect to the proton beam. The base-track efficiency is shown in Fig. 9 as a function of the film number in one of the most upstream configurations. The average base-track efficiency is higher than 90%. A slight decrease in the efficiency is observed in downstream configurations due to higher track density.

5 Interaction-vertices identification

Several thousands of proton interaction vertices are expected in a single target unit ($\sim 10^3$ cm^3). 400 GeV/c proton interactions produce on average more than ten charged particles and as many photons, having energies ranging from a few to tens of GeV. This results in a large number of secondary hadronic re-interactions and electromagnetic showers, that increases the number of reconstructed vertices up to two order of magnitudes. To set the scale, the unitary cell of the OPERA experiment [19, 20] contained in the same volume a single neutrino interaction vertex.

The analysis of the SHiP-charm emulsion data therefore required the development of dedicated software and analysis tools to extract the signal from an unprecedented background rate.

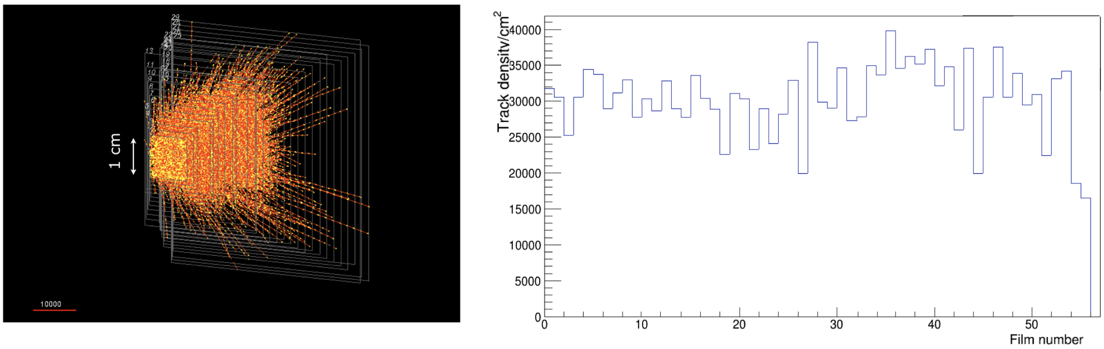

Figure 7: Left: tracks reconstructed in a 1×1 cm^2 of the configuration CHARM1-RUN6. Right: track density in one of the most downstream target units.

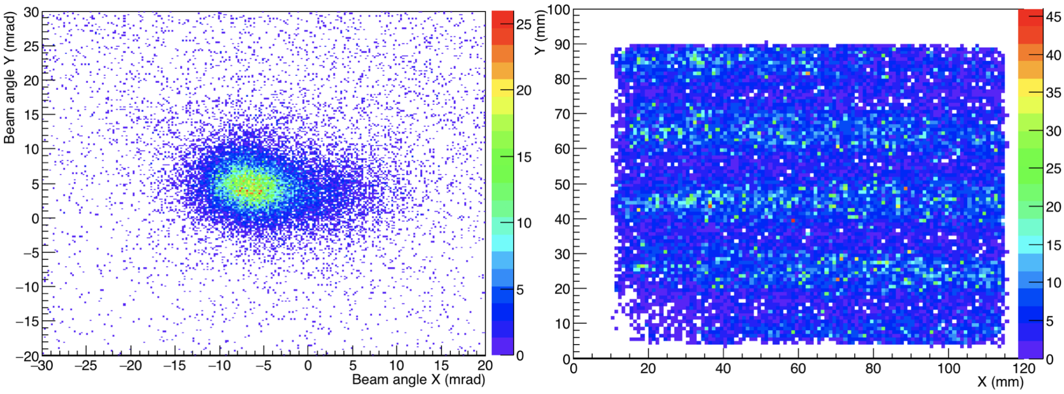

Figure 8: Left: angular dispersion of the proton beam as reconstructed in one of the exposed ECC target units. Right: position distribution of incoming protons on the emulsion surface.

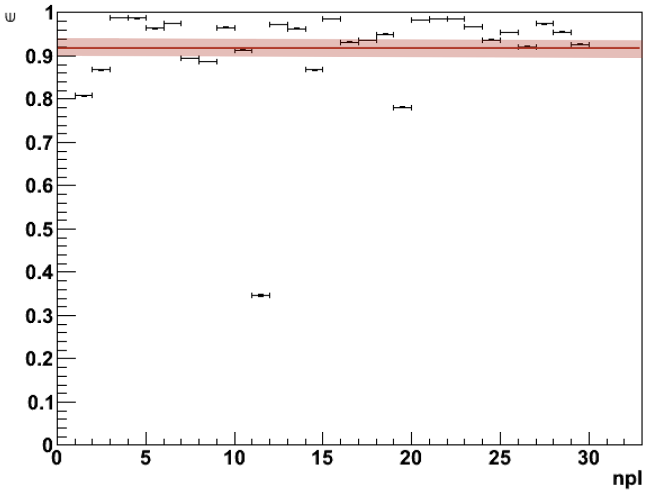

Figure 9: Film-by-film base-track efficiency for reconstructed protons in CHARM1-RUN2 configuration. The average efficiency, amounting to 92 ± 2 %, is shown as horizontal red line.

A full Monte Carlo simulation was performed in order to have a training sample that accurately reproduced data. The tracking and vertexing algorithms described in section 4 were applied both on simulated and real data. Distributions shown in Fig. 10 show that the simulation reproduces the data fairly well for multiplicities larger than six.

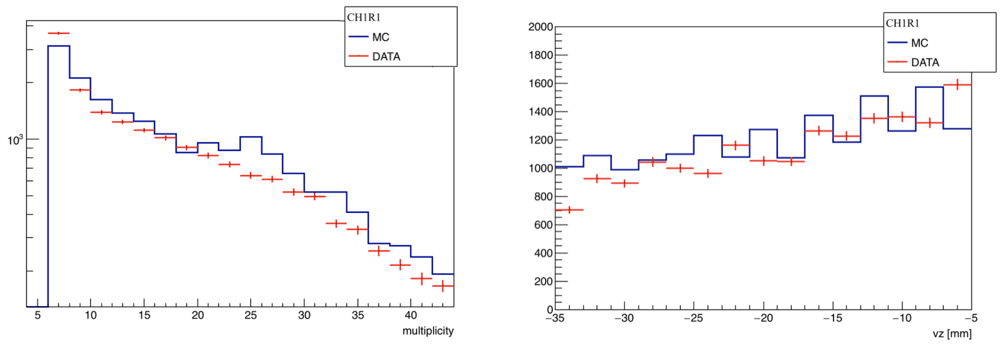

Figure 10: Charged track multiplicity (left) and position distribution along the beam axis (right) for vertices reconstructed in CHARM1-RUN1 configuration. Data points are shown in red, simulation is represented in blue. Distributions have been normalised to the number of p.o.t. integrated in the analised run.

A multivariate classification is performed using boosted decision trees from the TMVA toolkit [21] to distinguish the signal from a background with an unprecedented rate. The signal is made by interaction vertices while the background is mainly due to random association of low-momentum tracks and electromagnetic showers that crowd the ECC volume. Five discriminating variables were selected:

- vertex probability, as provided by the fit procedure

- angular distance between tracks associated to the vertex
- mean impact parameter of tracks at the vertex
- maximum impact parameter of tracks at the vertex
- fill factor of tracks at the vertex, defined as the ratio between the number of base-tracks building up the track and the number of emulsion films downstream of the vertex.

Left panel of Fig. 11 shows the above mentioned variables for the training sample. The output of the BDT ($V_{\rm bdt}$) is shown in the right panel of Fig. 11: a good separation between signal and background distributions is observed. The final selection of the signal component is performed on the variable R_{sel}, defined as the ratio between (1-$V_{\rm bdt}$) and the track multiplicity at the reconstructed vertex. The distribution of R_{sel} variable is shown in the left panel of Fig. 12 for data and simulation. The signal component is confined in the region $R_{\rm sel} < 0.1$, where a fairly good agreement between data and simulation is observed. The excess in the data for higher $R_{\rm sel}$ values is due to very low ($n < 4$) multiplicity vertices that are mainly made of random combination of instrumental background tracks. This background component, indeed, is not included in the current version of the simulation software.

The cut on the $R_{\rm sel}$ variable was optimised in order to maximise the background rejection while keeping an high signal selection efficiency. Both curves are represented in the right panel of Fig. 12, where the chosen cut is also shown. Vertices having $R_{\rm sel} < 0.05$ are classified as interaction vertices.

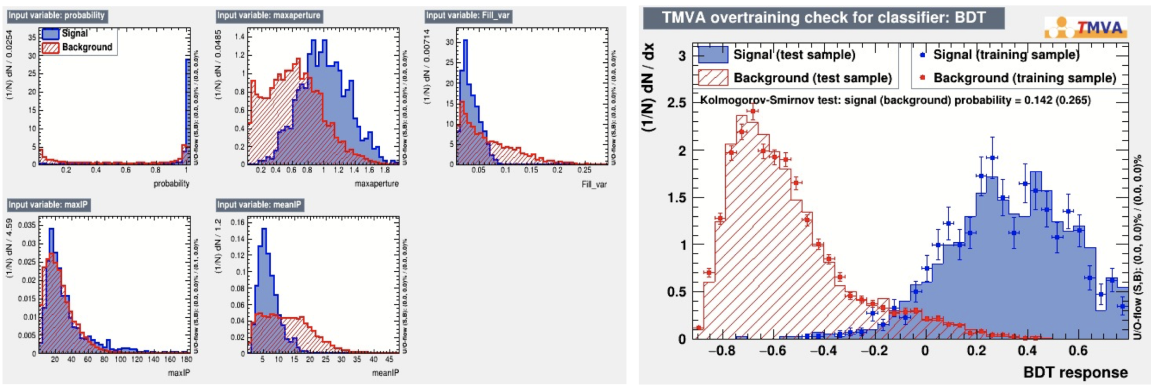

Figure 11: Left: distribution of input variables used in the multivariate analysis. Right: output value of the BDT for signal (blue) and background (red).

The angular distribution of tracks associated to interaction vertices is shown in Fig. 13. A good agreement is observed, both in normalisation and shape, thus validating the Monte Carlo simulation and the signal selection procedure.

The reconstructed position of interaction vertices along the beam direction for the most upstream and the most downstream configuration is shown in Fig. 14. The most upstream configuration shows very good agreement between data and Monte Carlo, both in normalisation and shape. A discrepancy between data is observed

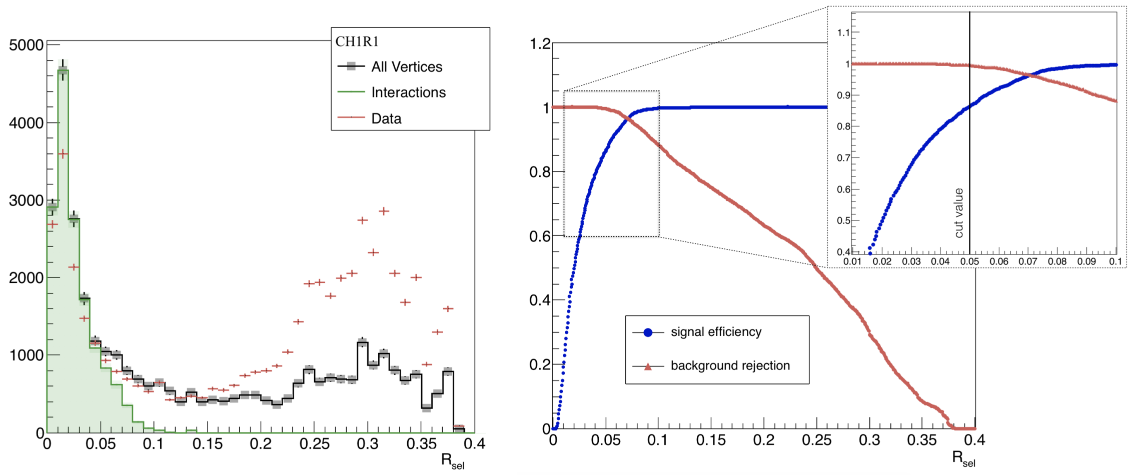

Figure 12: Left: distribution of the R_{sel} variable for data and simulated signal and background vertices. Right: signal efficiency and background rejection as a function of the R_{sel} cut.

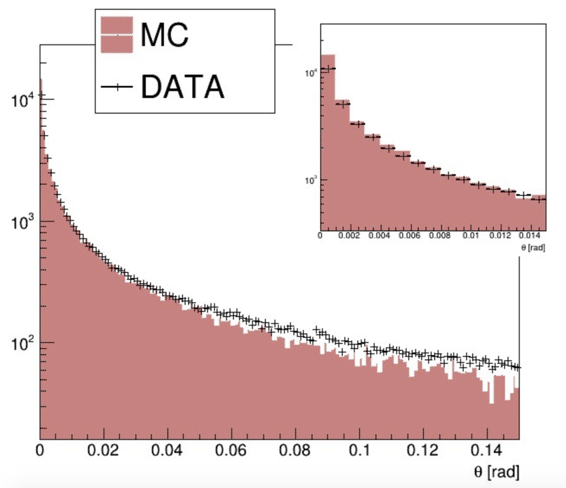

Figure 13: Angular distribution of tracks associated to interaction vertices. The inset shows the region with slopes smaller than 0.014 rad.

in downstream configurations and it is due to inefficiencies in track reconstruction that affect the overall number of selected vertex without introducing relevant biases in the variables that characterise interaction vertices.

The signal sample selected with the above mentioned procedure is made of two components: primary protons interaction vertices and hadron re-interaction vertices. A display of a Monte Carlo event containing both vertex categories is shown in Fig. 15.

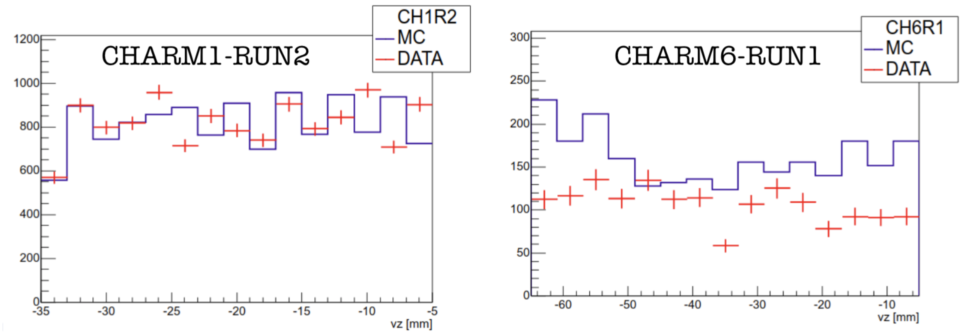

Figure 14: Vertex position along the beam direction for interaction vertices reconstructed in CHARM1-RUN2 (left) and CHARM6-RUN1 (right). Data and Monte Carlo distributions have been normalised to the number of p.o.t. integrated in the analised run.

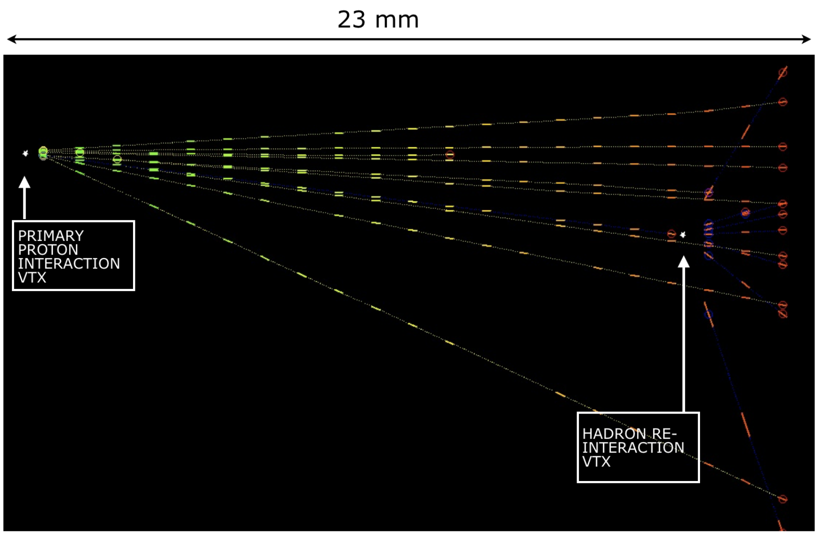

Figure 15: Display of a reconstructed Monte Carlo event where both the primary-proton interaction vertex and an hadron-reinteraction vertex are reconstructed.

The interaction vertex multiplicity for the most upstream and the most downstream configuration is shown in Fig. 16. The contribution of the primary proton and hadron-reinteraction components is shown separately. As one might expect, the hadron-reinteraction component increases as the configuration number increases, going from 11% in CHARM1 to 59% in CHARM6.

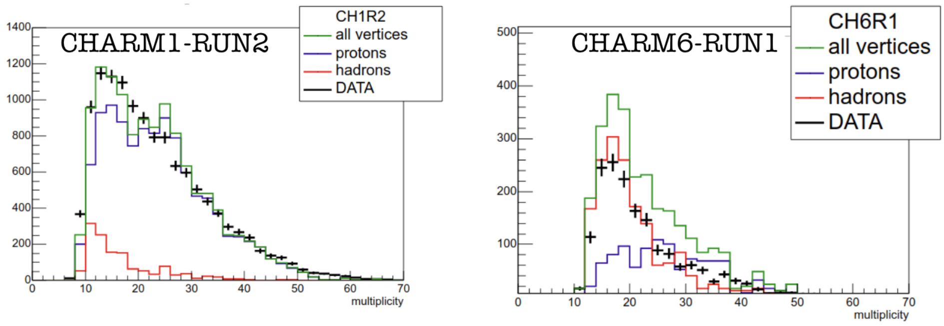

Figure 16: Charged track multiplicity for interaction vertices reconstructed in CHARM1-RUN2 (left) and CHARM6-RUN1 (right). Data and Monte Carlo distributions have been normalised to the number of p.o.t. integrated in the analised run.

The list of configurations used for the analysis described in this document is reported in Tab. 2 together with measured efficiencies. The observed fluctuations are related to different emulsion batches, handling procedures and chemical treatments used for the different runs.

Configuration	Efficiency (%)	Configuration	Efficiency (%)
CHARM1-RUN1	83	CHARM2-RUN4	55
CHARM1-RUN2	99	CHARM3-RUN1	70
CHARM1-RUN4	53	CHARM4-RUN1	38
CHARM1-RUN5	49	CHARM5-RUN1	51
CHARM2-RUN2	57	CHARM6-RUN1	66
CHARM2-RUN3	41		

Table 2: Vertex reconstruction efficiencies measured in the analised configurations.

6 Results

In order to merge data reconstructed in different configurations, inefficiencies were corrected by applying a normalisation factor, which also scaled all data to the same number of incoming protons on target.

By adding data reconstructed in different runs and combining the six configurations it is possible to retrieve the overall distribution of interaction vertices in a ∼365 mm long emulsion/lead target. The overall distribution is shown in Fig. 17 for data and simulation. Error bars on data points are obtained propagating the covariance matrix of the original histogram with the efficiency correction factor.

The distribution shown in Fig. 17 is made by the sum of two components: primary protons and hadron reinteractions. While the primary-proton component follows an exponential distribution, hadron reinteractions can be parametrised as a second-order polynomial. A Chi-square fit was therefore performed on data points with an exponential function and a 2^{nd} degree polynomial. The area under the two curves results to be 58% and 42%, respectively.

The slope of the exponential function provides an estimation of the proton interaction length in the emulsion/lead target of

$$\lambda_I^{\mathrm{meas}} = (182^{+19}_{-16})\ \mathrm{mm}.$$

This result is compatible with expectations from the full simulation, that predicts an interaction length of (175 ± 5) mm.

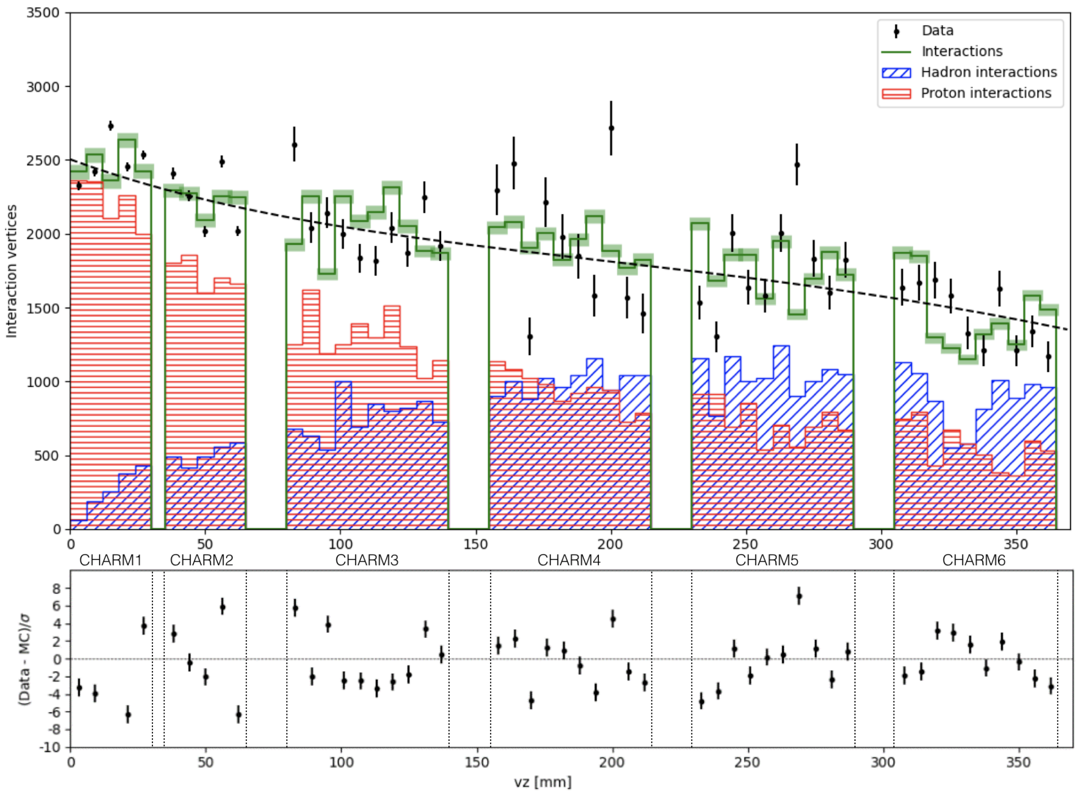

Figure 17: Position distribution of interaction vertices along the beam direction for data and Monte Carlo, merging results from the different configuration. Primary-proton and hadron-reinteraction components are shown in red and blue, respectively. Dashed line represents the fit to data points.

7 Conclusions

The analysis of the SHiP-charm emulsion data required the development of dedicated software and analysis tools to extract the signal from an unprecedented background rate. A good agreement between data and Monte Carlo expectations is found for the number of charged tracks defining the interaction vertex and the position of the vertex along the beam axis. These results prove the capability to reconstruct interaction vertices in a harsh environment.

The development of a Monte Carlo simulation that accurately described reconstructed data and the application of multivariate analysis techniques allowed to extract the primary proton interaction component in a $\sim$365 mm long emulsion/lead target and to evaluate the effective interaction length, that results to be in good agreement with expectations.

A Interaction-vertices characterisation

The reconstructed position of interaction vertices along the beam direction in the different runs of the six configurations are shown in Figs. 18, 19 and 20. Data and Monte Carlo distributions have been normalised to the number of p.o.t. integrated in each run.

The interaction vertex multiplicity for different runs is reported in Figs. 21, 22 and 23. The contribution of the primary proton and hadron-reinteraction components is shown separately. Data and Monte Carlo distributions have been normalised to the number of p.o.t. integrated in each run.

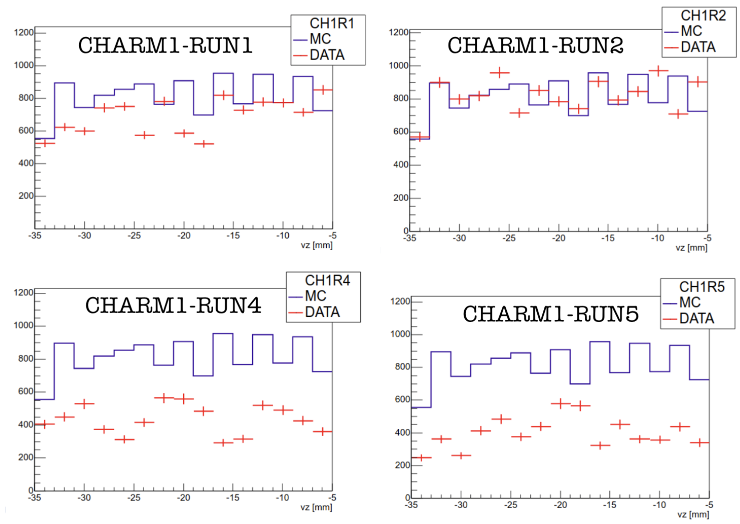

Figure 18: Vertex position along the beam direction for interaction vertices reconstructed in five runs of configuration CHARM1.

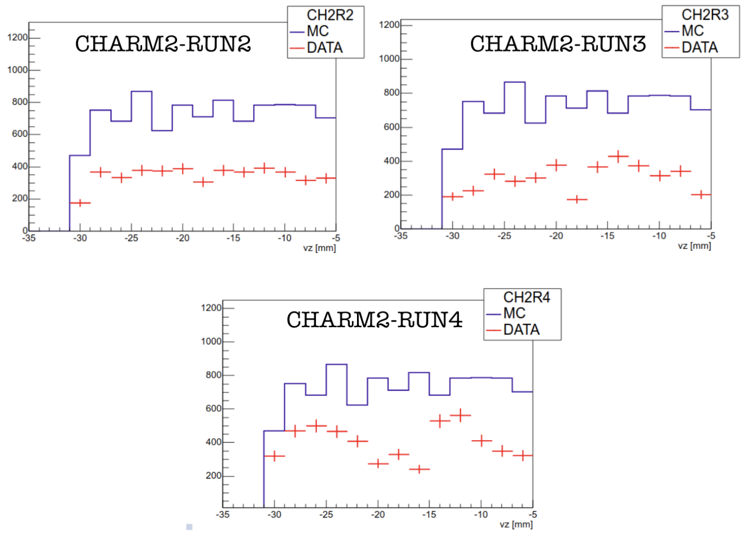

Figure 19: Vertex position along the beam direction for interaction vertices reconstructed in three runs of configuration CHARM2.

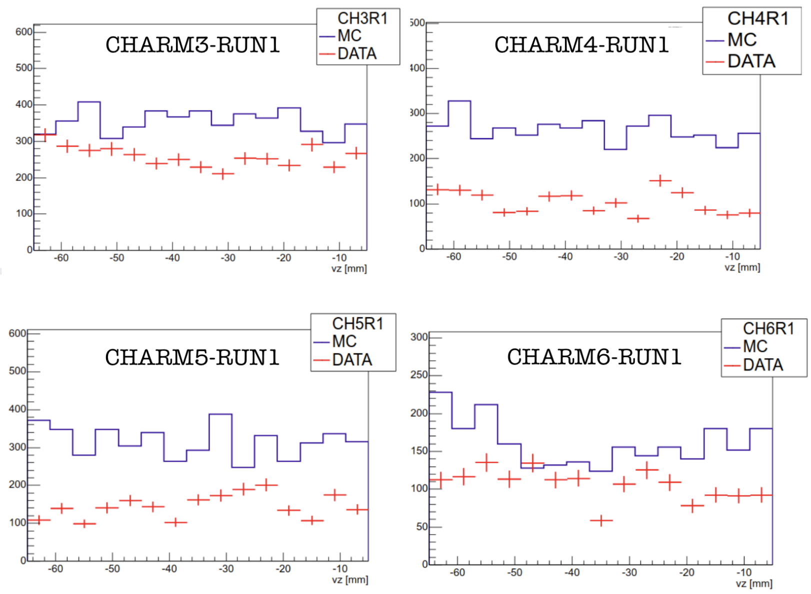

Figure 20: Vertex position along the beam direction for interaction vertices reconstructed in the first run of configurations CHARM3, CHARM4, CHARM5 and CHARM6.

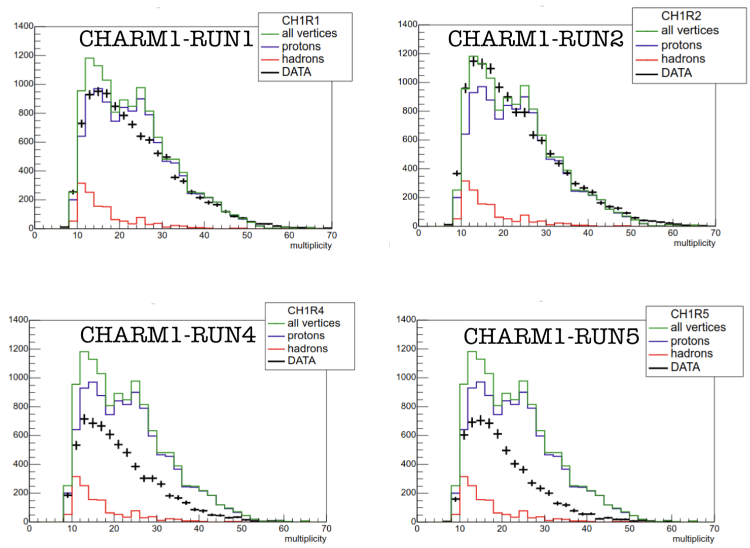

Figure 21: Charged track multiplicity for interaction vertices reconstructed in the five runs of configuration CHARM1.

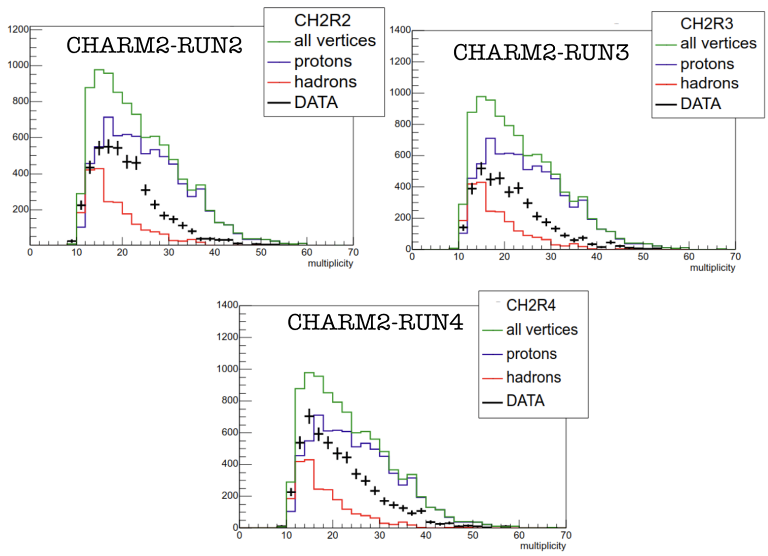

Figure 22: Charged track multiplicity for interaction vertices reconstructed in three runs of configuration CHARM2.

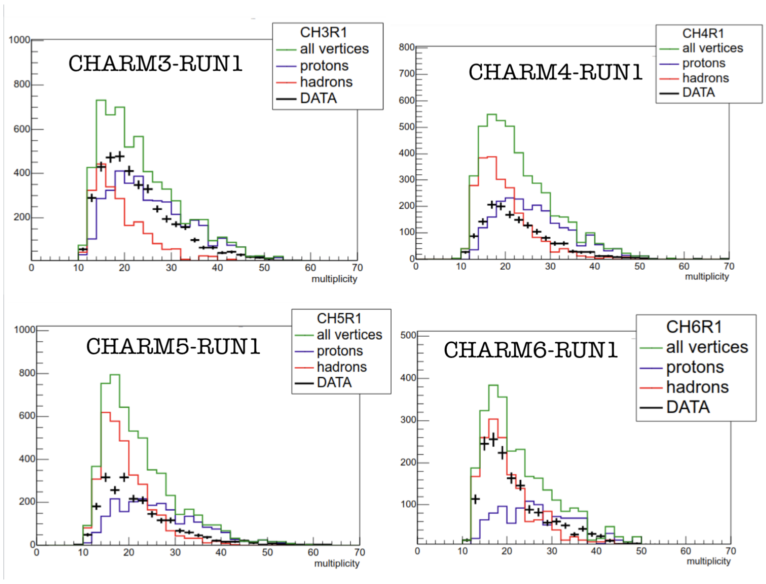

Figure 23: Charged track multiplicity for interaction vertices reconstructed in the first run of configurations CHARM3, CHARM4, CHARM5 and CHARM6.

References

[1] **SHiP** Collaboration, A. Akmete et al., *Measurement of associated charm production induced by 400 GeV/c protons*, Tech. Rep. CERN-SPSC-2017-033. SPSC-EOI-017, CERN, Geneva, Oct, 2017.

[2] **SHiP** Collaboration, M. Anelli et al., *A facility to Search for Hidden Particles (SHiP) at the CERN SPS*, [arXiv:1504.04956].

[3] M. Rosenthal, N. Charitonidis, P. Chatzidaki, R. Margraf, H. Wilkens, F. Bergsma, and P.-A. Giudici, *Magnetic Field Measurements of the GOLIATH Magnet in EHN1*, Tech. Rep. CERN-ACC-NOTE-2018-0028, Mar, 2018.

[4] **ATLAS IBL** Collaboration, B. Abbott et al., *Production and Integration of the ATLAS Insertable B-Layer*, *JINST* **13** (2018), no. 05 T05008, [arXiv:1803.00844].

[5] M. Garcia-Sciveres et al., *The FE-I4 pixel readout integrated circuit*, *Nucl. Instrum. Meth. A* **636** (2011) S155–S159.

[6] T. Beattie et al., *Light yield of Kuraray SCSF-78MJ scintillating fibers for the Gluex barrel calorimeter*, *Nucl. Instrum. Meth. A* **767** (2014) 245–251.

[7] R. Zimmermann, J. Ebert, C. Hagner, B. Koppitz, V. Savelev, W. Schmidt-Parzefall, J. Sewing, and Y. Zaitsev, *The precision tracker of the OPERA detector*, *Nucl. Instrum. Meth. A* **555** (2005) 435–450. [Erratum: Nucl.Instrum.Meth.A 557, 690 (2006)].

[8] M. Al-Turany, D. Bertini, R. Karabowicz, D. Kresan, P. Malzacher, T. Stockmanns, and F. Uhlig, *The FairRoot framework*, *J. Phys. Conf. Ser.* **396** (2012) 022001.

[9] **GEANT4** Collaboration, S. Agostinelli et al., *GEANT4–a simulation toolkit*, *Nucl. Instrum. Meth. A* **506** (2003) 250–303.

[10] L. Arrabito et al., *Track reconstruction in the emulsion-lead target of the OPERA experiment using the ESS microscope*, *JINST* **2** (2007) P05004, [arXiv:0705.3102].

[11] V. Tyukov, I. Kreslo, Y. Petukhov, and G. Sirri, *The FEDRA Framework for emulsion data reconstruction and analysis in the OPERA experiment*, *Nucl. Instrum. Meth. A* **559** (2006) 103–105.

[12] R. Brun, F. Rademakers, and S. Panacek, *ROOT, an object oriented data analysis framework*, in *CERN School of Computing (CSC 2000)*, pp. 11–42, 2000.

[13] N. Armenise et al., *High-speed particle tracking in nuclear emulsion by last-generation automatic microscopes*, *Nucl. Instrum. Meth. A* **551** (2005) 261.

[14] L. Arrabito et al., *Hardware performance of a scanning system for high speed analysis of nuclear emulsions*, *Nucl. Instrum. Meth. A* **568** (2006) 578, [physics/0604043].

[15] N. Armenise et al., *High-speed particle tracking in nuclear emulsion by last-generation automatic microscopes*, *Nucl. Instrum. Meth. A* **551** (2005) 261.

[16] A. Alexandrov et al., *A new generation scanning system for the high-speed analysis of nuclear emulsions*, *JINST* **11** (2016), no. 06 P06002.

[17] A. Alexandrov et al., *A new fast scanning system for the measurement of large angle tracks in nuclear emulsions*, *JINST* **10** (2015), no. 11 P11006.

[18] A. Alexandrov et al., *The Continuous Motion Technique for a New Generation of Scanning Systems*, *Sci. Rep.* **7** (2017), no. 1 7310.

[19] R. Acquafredda et al., *The OPERA experiment in the CERN to Gran Sasso neutrino beam*, *JINST* **4** (2009) P04018.

[20] **OPERA** Collaboration, N. Agafonova et al., *Final results of the search for $\nu_\mu \to \nu_e$ oscillations with the OPERA detector in the CNGS beam*, *JHEP* **06** (2018) 151, [arXiv:1803.11400].

[21] H. Voss, A. Hocker, J. Stelzer, and F. Tegenfeldt, *TMVA, the Toolkit for Multivariate Data Analysis with ROOT*, *PoS* **ACAT** (2007) 040.